Development of Instrumentation for the Analysis of Photoconductivity in Functional Materials

Brandon L. Chapman, Advisor: Dr. Janice Musfeldt

Abstract

Photoconductivity as a process is useful in probing the behavior of charge carriers in materials, analyzing behavior in band gap regions with high absorbance values, and in analysis of materials that are physically brittle or non-optimal for traditional spectroscopic analysis. In spite of these benefits, instruments for measuring these properties are not commonly manufactured. A graduate student in the Musfeldt Lab prototyped a rudimentary instrument for measuring photoconductivity in materials using a broadband source, bandpass filters, various optical components, and a combined voltage source/picoammeter coupled with Labview interfaces designed to control the parameters of the electrical current supplied to the sample. However, due to the usage of sputtered Au contacts and tungsten leads as a method of establishing electrical contact, the choice of broadband source, signal produced by the instrument suffered from a lack of stability and was hindered by the decay of contact over time. This thesis explores the benefits of using solid, silver epoxy contacts as well as other improvements, discusses possible methods for further improving/developing the instrument, and

Introduction

Photoconductivity was first observed in 1873 when it was discovered that the electrical resistance of pure selenium semiconductors was dependent on ambient light, leading to the development of early light sensors and initiating research into the physics behind the process of photoconductance. This property manifests via the mechanism of excitation of electrons in the

material, resulting in the generation of charge carriers, with the properties of the material determining the types of charge carriers and the energies required for excitation. While all materials have a base level of conduction/resistivity, only certain materials have a band structure that correlates to a band gap within range of photoexcitation but beyond thermal excitation of electrons from valence/non-conducting bands into conducting bands. In intrinsic semiconductors such as silicon and selenium, an electron is excited from the valence band into the conduction band, generating a flowing electron and a corresponding hole which behaves similarly to a particle, the combination of which is referred to as an exciton (see Fig. 1 (top)). This can further be divided into direct and indirect excitation processes, with direct band gaps using only excitation energy from incident radiation, whereas indirect band gaps utilize energy contributed from the lattice of the crystal. In *n*- and *p*-type semiconductors this process is also present but is less energetically favored than the excitation of donor electrons into the conduction band in n-type semiconductors and the excitation of electrons in the valence band into acceptor energy levels. Either of these processes differs from the intrinsic process in that only one form of free charge carrier is generated, with electrons being produced in *n*-type semiconductors and holes in *p*-type semiconductors (see Fig. 1 (bottom)).[1,8]

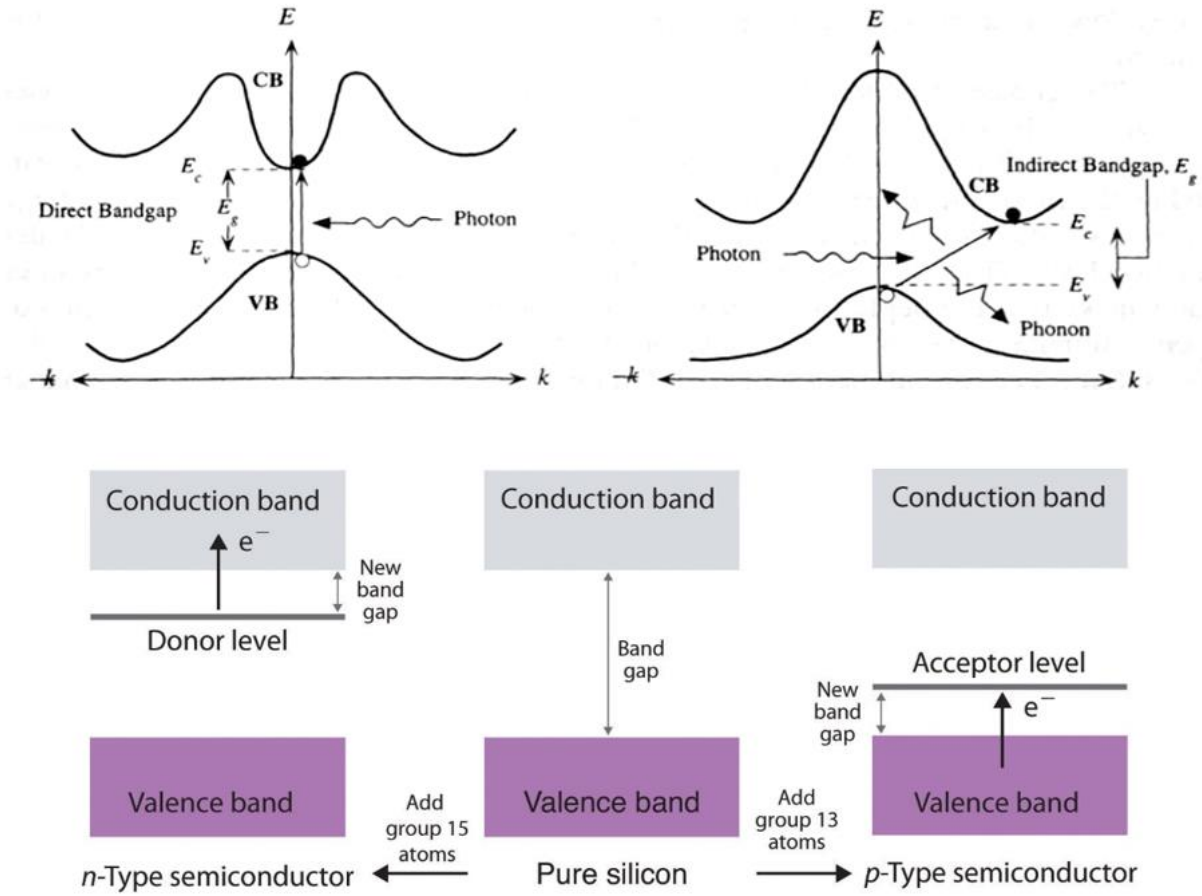

Fig. 1: *(top) Diagram of simple band gap transitions,*[4] *(bottom) Diagram of excitation processes in doped semiconductors.*[2]

As photoconductivity manifests as a result of excitation processes, it is proportional to the absorbance of the material and can provide a window into the optical properties of the material as well as the behavior of electrons under various conditions. However, as the effect is dependent on the presence of additional carriers, it is only measureable prior to recombination and is thus dependent on mechanisms of recombination and trapping. This also incorporates effects on the movement of carriers through the material, including various fields and the local concentrations of carriers. T. S. Moss separates the wide array of possible measurements into three categories: homogeneous materials with no applied electric field, homogeneous materials with applied electric field (traditional photoconductivity), and materials with internal *p-n* junctions with no

external electric field (photovoltaics). Further, these measurements can be divided into steady-state photoconductivity (SSPC) and transient photoconductivity (TPC) based upon the desired properties to be probed, with possibilities including the behavior of charge carriers (i.e. trapping of carriers in the crystal lattice or quenching of carriers by various mechanisms), band structure of the material, and, by extension, the absorbance of the material. While SSPC analyses properties at the equilibrium state of the material in question, TPC probes time-dependent processes in the material to determine other properties of the material. For sake of relevance, only SSPC will be discussed, as programs for analysis of time-dependent data are not available for original instrumentation due to significant high-frequency, short lifetime noise present in time dependent data.[1,9]

In SSPC, a monochromatic source generates charge carriers in the form of exciton pairs via absorption in a sample, creating a change in available charge carriers as described by the equation $\Delta\sigma = \sigma_{PC} = e(\mu_n \Delta n + \mu_p \Delta p)$, where e is the charge of an electron, μ refers to the mobility of charge carriers, and Δn/p are the change in concentration of charge carriers. In this work, conduction occurs primarily across the surface of the sample, as electrical contact is accomplished on the illuminated surface, and most samples have high absorption coefficients across all measured wavelengths. In most materials, the overall mobility of carriers is drastically dominated by one of the two mobility terms, reducing the mathematics to consider only one of the carriers. Generation of carriers can be simplified to Gτ, where G is the rate of generation of free carriers and τ is the average lifetime of carriers, resulting in the equation $\sigma_{PC} = eG\mu$, with G being described as $\eta\left(\frac{I_0}{h\nu}\right)(1-R)\left(\frac{1-\exp(\alpha d)}{d}\right)$, where η is the quantum efficiency of the excitation process, I_0 is the intensity of incident radiation, $h\nu$ is the energy of a photon, R is the reflection coefficient of the sample, α is the absorption coefficient of the sample, and d is the

sample thickness. As η, R, and α are dependent on the wavelength of incident photons, monochromatic light allows for the scanning of photoconductive processes across an energy scale. As αd << 1 in most samples, the G equation can be reduced to $G \cong \eta\left(\frac{I_0}{hv}\right)(1-R)\alpha$. From this, the proportionality between photocurrent and optical absorbance can be determined to be $\sigma_{PC} \propto G\tau = \eta\alpha(E)\tau\left(\frac{I_0}{hv}\right)(1-R)$, with η, τ, and all other factors behaving as scalars.[1,5,9] This proportionality indicates that the resulting data when plotted against the energy of incident radiation will resemble the corresponding absorbance spectrum of the sample.

While measurement of photoconductivity can provide a window into other previously discussed properties of a material, it can also allow for band gap analysis over a range beyond what is available to traditional absorbance and reflectance methods. As the process is not dependent on the availability of a measurable signal of light after the sample is irradiated, the need for detectors and amplification of signal is eliminated. Hypothetically, if transmitted/reflected light could be directed towards a detector in a photoconductivity instrument, spectra could be used to obtain a better understanding of the electronic structure of the material. While there remains a need for a stable source of light over a certain bandwidth and a plausible method by which current can be passed through the sample without interference from outside stimuli, these constraints are far easier to surmount.

For samples with rather large absorbance values at a given wavelength such as candidates for solar cells or air sensitive materials which are unable to be cleaved or deposited as thin films while maintaining the desired crystal structure, photoconductivity can allow for the effective measurement of band gaps whereas no other technology could. This is particularly true if polishing/thinning the sample are effectively impossible due to extreme fragility in the bulk state

or at the thickness required for measurement of traditional transmission. An example of such a material is $CsSnCl_3$, a semiconductor with strong absorption bands which undergoes a temperature driven phase transition which is also catalyzed by atmospheric water vapor.[11] Further, the application of a magnetic field can also be incorporated into standard photoconductivity for the investigation of magnetoresistance as well as the coupling of photoconductive and magnetoresistive processes.

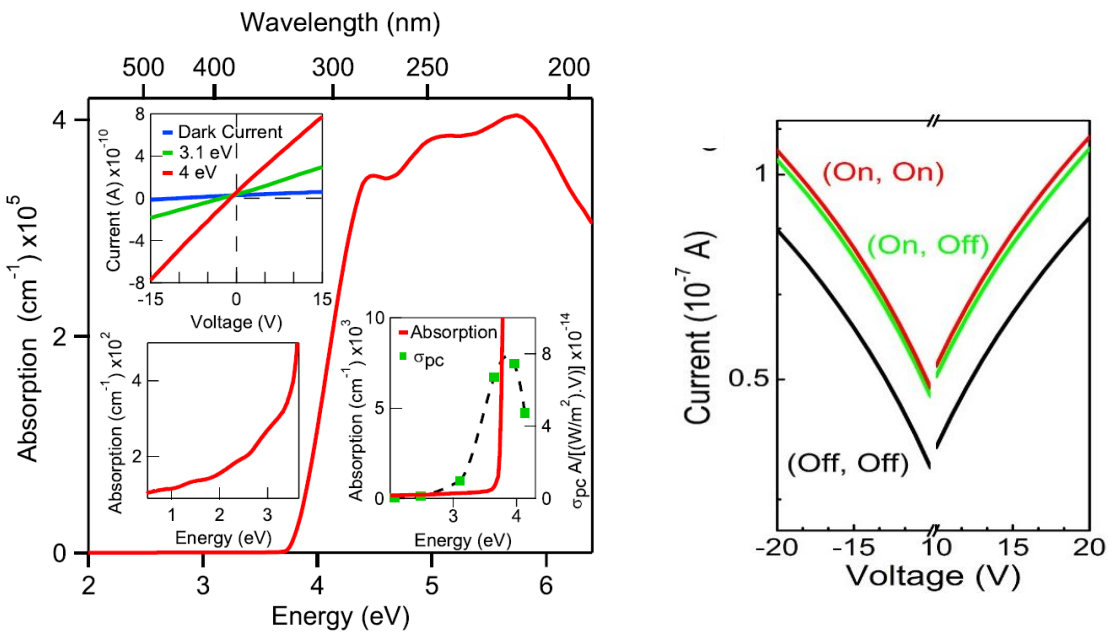

Fig. 2: *(left) Photoconductivity and absorption data on $CsSnCl_3$[11] (right) Comparison of I-V data under illumination/application of field*

In lieu of the benefits of photoconductivity over standard reflectance and absorbance spectroscopies, a previous graduate student designed and tested an instrument for measuring the photoconductivity of solid crystals. This apparatus can be seen in a schematic view below.

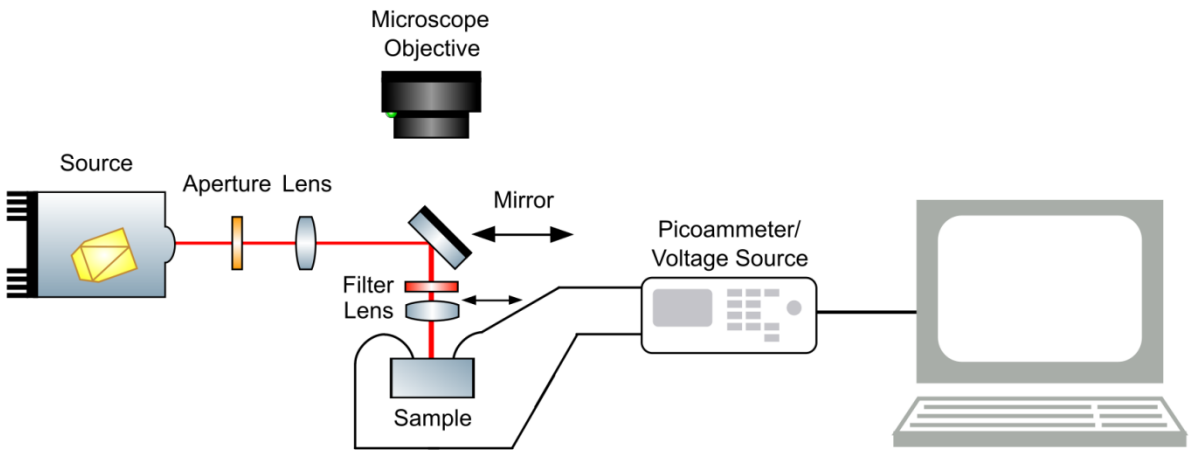

Fig 3.: *Diagram of Original Photoconductivity Instrument*

Specifically, the instrument used a halogen white light source followed by an aperture to cut down the beam from its original conical shape to smaller, more collimated beam, a lens to fully collimate the beam, a 90-degree ellipsoid mirror to redirect the beam towards the sample, and a lens to focus the beam onto the sample, with a position for placing a filter of the user's choice prior to the focusing of the beam for sake of long-term preservation of filters. Shown below is a table of the available bandpass filters for this setup, with other neutral density filters available for power-dependent measurements, although these are rarely used due to the possibility of varying the intensity of incident light by controlling the voltage supplied to the bulb from the power source.

Filter center wavelength (nm)	FWHM (nm)	Energy (eV)	Blocked range (nm)	T_{min} (%)	Seller
2000	500±100	0.62	200–12000	70	Thorlabs
1500	12±2.4	0.83	200–1850	70	Thorlabs
1250	10±2	0.99	200–3000	70	Thorlabs
1000	10±2	1.24	200–3000	70	Thorlabs
900	40±8	1.38	200–1150	70	Thorlabs
800	40±8	1.55	200–1150	70	Thorlabs
700	40±8	1.77	200–1150	70	Thorlabs
650	40±8	1.91	200–1150	70	Thorlabs
600	40±8	2.06	200–1150	70	Thorlabs
550	40±8	2.25	200–1150	70	Thorlabs
500	40±8	2.48	200–1150	70	Thorlabs
400	40±8	3.09	200–1150	45	Thorlabs
380	10±2	3.26	200–3000	25	Thorlabs
360	10±2	3.44	200–3000	25	Thorlabs
340	10±2	3.65	200–3000	25	Thorlabs
313	10±2	3.96	200–10000	15	Edmund Optics
300	10±2	4.13	200–10000	15	Edmund Optics
280	10±2	4.43	200–10000	12	Edmund Optics

Table 1: *Table of Available Bandpass Filters*

Samples were prepared by sputtering 250 micron spots in a square grid pattern to enhance the conduction of electricity into the crystal lattice, and tungsten leads were positioned on two adjacent spots using micropositioners before current was supplied from a Keithley Picoammeter/Voltage Source.

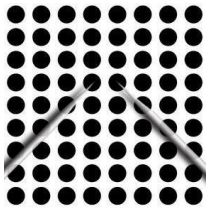

Fig. 4: *Diagram of Original Contact Method*

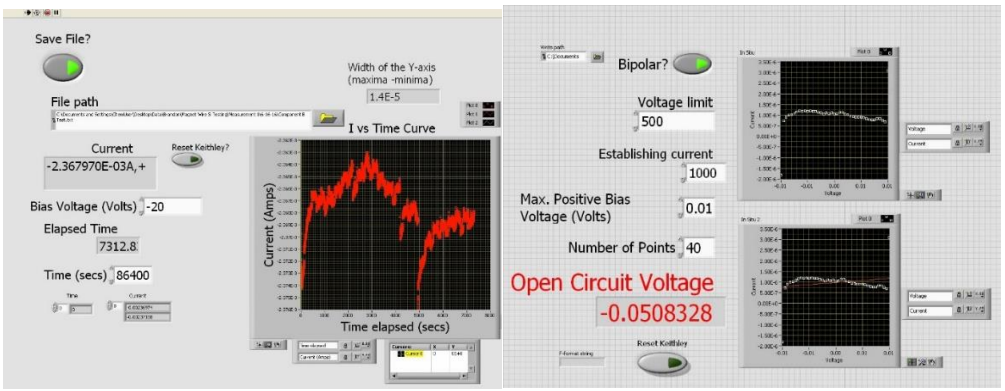

Fig. 5: *(left) Time Dependance Interface, (right) I-V Interface*

The picoammeter is controlled using two LabVIEW interfaces originally designed along with the original configuration of the instrument. The first program measures the current across the system at a given voltage over a set period of time, while the second measures the current across the system over a range of voltages. The Time Dependence interface allows for the specification of a file save path, voltage, and length of measurement, all of which must be specified prior to collecting data. Other options include whether the file is to be saved (unnecessary in quick trial runs) and whether to reset the voltage source at the beginning of the measurement, which should be done if it has been powered off since the previous measurement. As data is collected, it is added to the graph on the right side of the interface. Rescaling is

accomplished by unlocking the axes and using the selection tool to specify a range graphically or by double clicking the maxima/minima of an axis and inputting the desired value. This is useful for estimating magnitudes of changes in signal, as the y-axis can be resized to the edges of the feature to be measured and the size will be shown on the readout above the graph. It is important to note two details about how the program saves and displays data: collected information is automatically appended to the text file specified in the file path, and data will continue to be displayed between measurements unless the arrays below the Time panel are right-clicked, Data Operations is selected, and Empty Array is performed. This will not remove the information from the graph until measurement is started, and cannot be done during measurement. Both programs are limited by the capabilities of the Keithley Voltage Source/Picoammeter, which are summarized in the table below.

RANGE	5½ DIGIT DEFAULT RESOLUTION	ACCURACY (1YR) [1] ±(% RDG. + OFFSET) 18°–28°C, 0–70% RH	TYPICAL RMS NOISE [2]	TYPICAL ANALOG RISE TIME (10% TO 90%)[3] DAMPING[4] OFF	ON
2 nA	10 fA	0.3 % + 400 fA	20 fA	4 ms	80 ms
20 nA	100 fA	0.2 % + 1 pA	20 fA	4 ms	80 ms
200 nA	1 pA	0.15 % + 10 pA	1 pA	300 µs	1 ms
2 µA	10 pA	0.15% + 100 pA	1 pA	300 µs	1 ms
20 µA	100 pA	0.1 % + 1 nA	100 pA	110 µs	110 µs
200 µA	1 nA	0.1 % + 10 nA	100 pA	110 µs	110 µs
2 mA	10 nA	0.1 % + 100 nA	10 nA	110 µs	110 µs
20 mA	100 nA	0.1 % + 1 µA	10 nA	110 µs	110 µs

Table 2: *Sensitivity of Keithley 6487 Voltage Source/Picoammeter*[6]

The I-V interface allows for the specification of a file path, maximum voltage, establishing current, maximum voltage for measurement, and the number of data points to be collected. Further, there are two Boolean switches for indicating whether the voltage source will be reset prior to measurement (generally not desired) and whether the measurement will take

place over both positive and negative voltages. The Voltage Limit is a safety mechanism which prevents excessive current from damaging the device, and the Max. Positive Bias Voltage specifies the maximum voltage the system will collect data. If Bipolar is selected, the system begins collecting data at the voltage specified in Max Positive Bias Voltage, but in the opposite polarity, or at a negative voltage, and then progresses through the origin and into positive voltages. For collecting data at a particular resolution, the number of points required to accomplish said resolution must be calculated. Graphs on the right of the I-V interface can be interacted with identically to the graph in the Time Dependence program to investigate data, with the lower graph approximating and plotting a linear fit to the collected data after all data is collected. At the end of each measurement, the program will prompt the user to determine whether the data is to be saved, and to input a label to the data set. It will then save three files, each with the specified label and an appended label indicating what data is stored: -IV.txt being the collected data, -linear fit.txt the calculated points at each voltage corresponding to the linear fit, and Voc.txt the open circuit voltage.

By measuring the current across a sample under no direct illumination across several voltages, illuminating the sample, repeating the measurement, subtracting the dark current from the collected values, and correcting for the variation in power density between wavelengths, σ_{PC} can be determined and compared to available reflectance/absorbance spectra for verification. However, due to several complications resulting in variations in collected data, several improvements were made to increase the viability of measurement.

Experimental

The usage of a halogen lamp coupled with a power controller allowed for the use of filters across a wide range of wavelengths due to the wide emission band of the lamp, but was

ultimately a source of noise in and of itself. Flickering of the bulb, a large angle of emission, and the presence of a fan on the lower mount of the lamp contributed heavily to variations observed when measuring the change in current over time ($\Delta\sigma(t)$) and, when of a large enough magnitude, was also visible in current vs. voltage measurements. Due to properties of the method of contact, vibrations caused by the fan lead to several other issues related to the use of tungsten leads but will be discussed later. Of primary interest was the ability to focus the beam on a small point, drastically increasing the power density available at a given wavelength and generating larger, faster responses in samples, as an increased power density allows for a larger measured response in a material, allowing for measurement of photoconductivity in samples with little response and increasing the signal to noise ratio in all measurable samples. This was prevented by a lack of homogeneity of the beam along with the wide angle of emission. As a result, the source was replaced with a xenon arc lamp, resulting in a large reduction in overall output, but drastically increasing the homogeneity of the beam and reducing the angle of emission such that the achieved focal point was small enough to more than account for the decreased power.

Due to many sources of vibration, tungsten probes coupled with sputtered gold leads resulted in poor reproducibility of measurements, unreliability of data, and limited the types of samples which could be measured. Given that the probes were essentially needles, samples that were not overly durable risked being severely damaged if probes were lowered too quickly and often degraded at a higher rate than the gold contacts due to movement of the needles across the surface. As the probes were connected to ~4 in brass arms before connection to the voltage source, any vibrations present in the optics table were magnified before reaching the probes, resulting in large (on the scale of the contacts) movements and, by extension, variations in the quality of contact between the voltage source and the sample. This resulted in a need to hurry

measurements due to the eventual wearing down of contacts and a visible degradation in conductivity over time. While the original instrumentation was placed on a floated table to remove coupling of the effects of the previously mentioned fan were magnified, and the table was only designed to eliminate high frequency vibrations. This left the system as a whole sensitive to any variety of motion within ~25 feet of the instrument, including movements outside the lab itself.

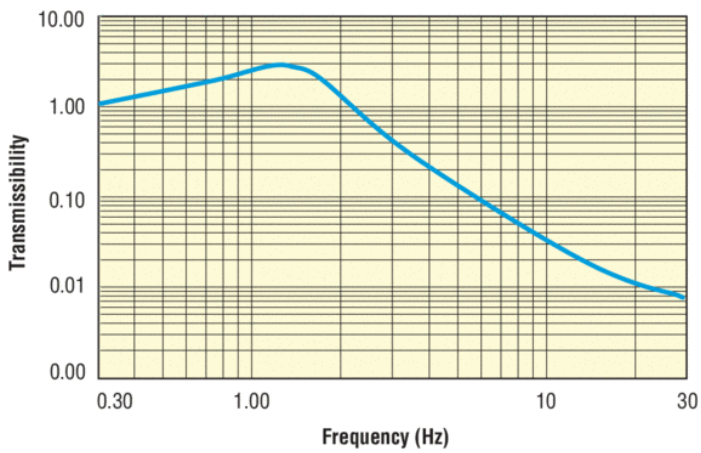

Fig. 6: *Frequency spectrum of a similar Newport damping table*[14]*, with the damping ratio given by the equation* $\zeta = \frac{c}{2\sqrt{km}}$.[13] *Note that the dampening frequency is inversely proportional to mass.*

In an attempt to limit this, the second source for the instrument was installed with a more modern fan with a much smaller magnitude of vibration and the instrument was redesigned on a larger optics table isolated from the ground via foam padding. Prior to any testing of the finalized setup, a power spectrum was taken by focusing the beam on a power meter and dividing the determined power by the average radius of the beam spot, resulting in a power spectrum which accounted for the loss of photons across each optical component.

To further reduce noise, the method of contact was modified from using tungsten needles to applying a conductive silver epoxy to the surface of a sputtered sample and affixing 75 micron

copper wire with a ~5 micron amidester coating.[10] This eliminated issues of reproducibility and drastically reduced the need for reduction of vibration beyond need for realignment of optics and wearing of electrical contacts in the system. This method increases the time necessary for preparation, as the epoxy must be prepared rather carefully and cured overnight in a vacuum oven, but the significant reduction in noise and improvement of overall current more than account for the disadvantages of sample preparation. This was refined to allow for sample preparation to take place over the course of a single day by developing a procedure which required only a single batch of epoxy to be prepared and cured overnight. However, during testing it was determined that simple crimping and soldering were inefficient methods of joining the wires to the voltage source. This was due to the surprisingly high impedance of the single-layer amidester coating used to prevent damage to the wire. While the coating was removed at each end of the wire as part of cutting to the desired length, allowing current to flow, a method of stripping this coating was investigated and determined to be, within practical cost constraints, to be careful application of heat from a controlled flame by bringing the wire just close enough to the flame that the coating was heated to its flash point followed by mechanical removal of copper oxide and polymer residue via fine-grit sandpaper.

To fully solidify contact, the technique was further refined to include the attachment of a two-pin electrical connector to the glass slide holding the sample and using the silver epoxy to eliminate all visible reliance on non-solid contact between two components of the circuit. The chosen connector was rated to 250 V for sake of limiting the size of the prepared sample, as the current sample stage had been designed for the measurement of photomagnetoresistance. The sample was then affixed using adhesive to the sample stage to prevent any change in physical location due to vibration or tension on the wires leading to the connector. As a precaution for

vibrational shifting of the sample from the sample area, adhesive is applied to the surface of the aluminum stage before affixing the sample slide. Total solidification of electrical contacts also has the added benefit of eliminating the need for movement of optical components for alignment of sample, further increasing reproducibility and eliminating need for periodic adjustment of optics to maintain proper focus on the sample.

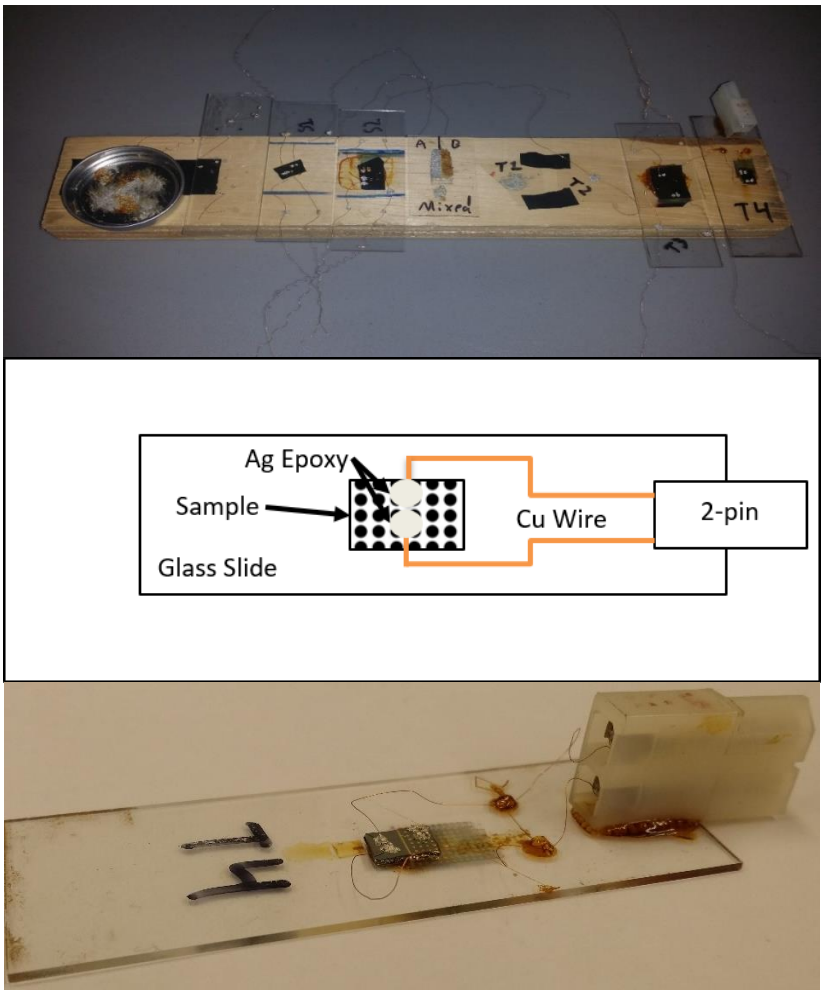

Fig 7: (top*) Progression of Ag epoxy usage (organized chronologically left to right) (middle) Diagram of final sample preparation method (bottom) Closeup of final sample configuration*

In collaboration with other students, a device for the measurement of photomagnetoresistance was prepared using an optical rail system. A mounting system was designed which allowed for the interfacing of the track to the optical table, and polymer

enclosures for rare-earth magnets were designed. Using a micrometer, the distance between the magnets could be varied from several inches to the thickness of the center sample location, with the thinnest practical stage design currently being ~1/4”. Due to the strength of the attractive forces between the magnets, the danger of damaging the track was addressed by using nylon-tipped set screws to anchor each component to the track. Further, during measurement it was determined that reflection of stray light from the surface of the magnets was a source of abnormally high photoconductance, which was eliminated by coating with black paint.

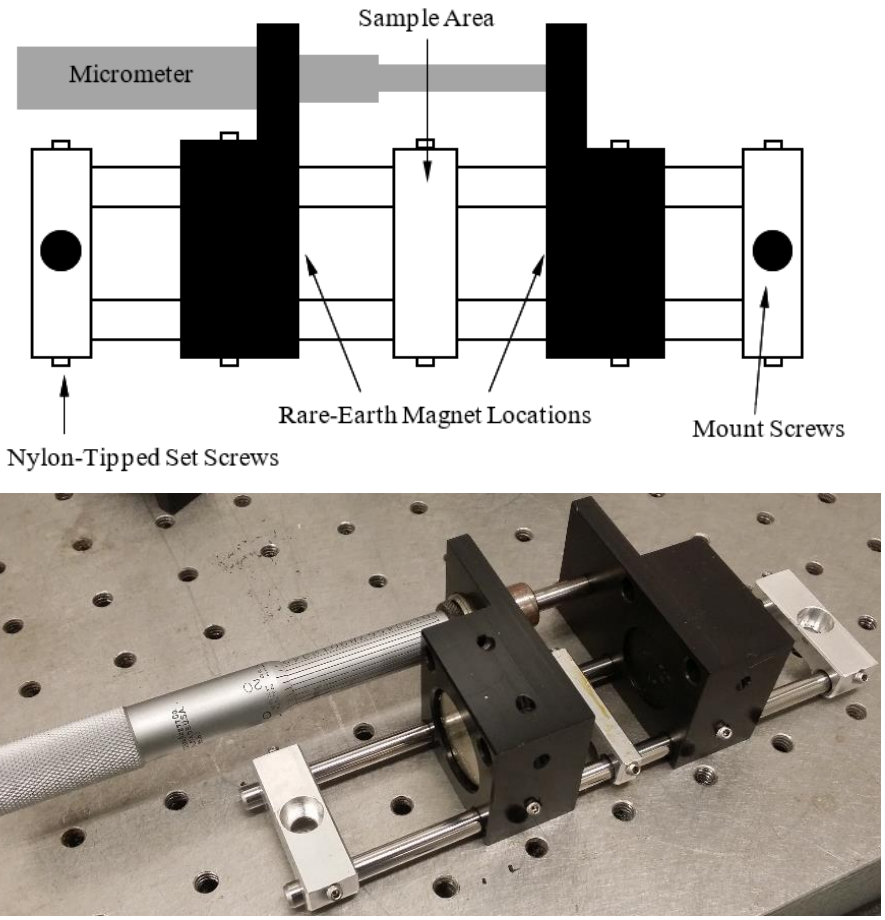

Fig 8: *Photomagnetoconductance attachment*

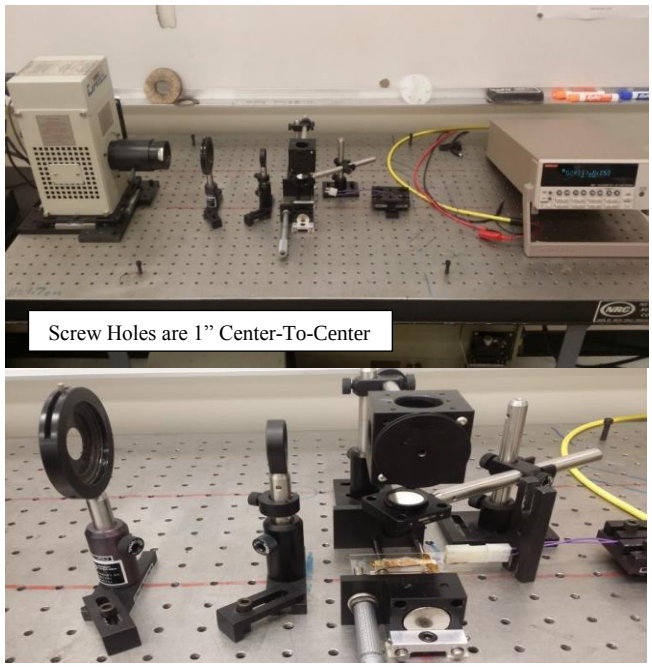

Fig. 9*: (top) Completed photoconductivity instrument, (bottom) close-up of final optical configuration*

Results & Discussion

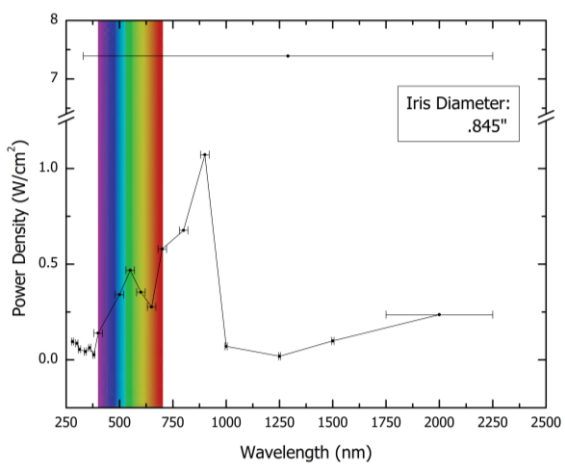

Fig. 10: *Power density of beam through each bandpass filter*

Due to the natural spectrum of the xenon arc lamp, differential transmission through optical components, successive back reflectance of the beam between optical components, and variation in the bandwidth of filters, power density is significantly variant across λ. The iris prior to beam collimation is used to eliminate some light at non optimal incident angles, giving a more

prominent beam spot. Wavelengths outside the visible spectrum and without significant leakage of light in the visible range must be assumed to have a spot size similar to the last filter with significant leakage of visible light, which is the 100 nm filter.

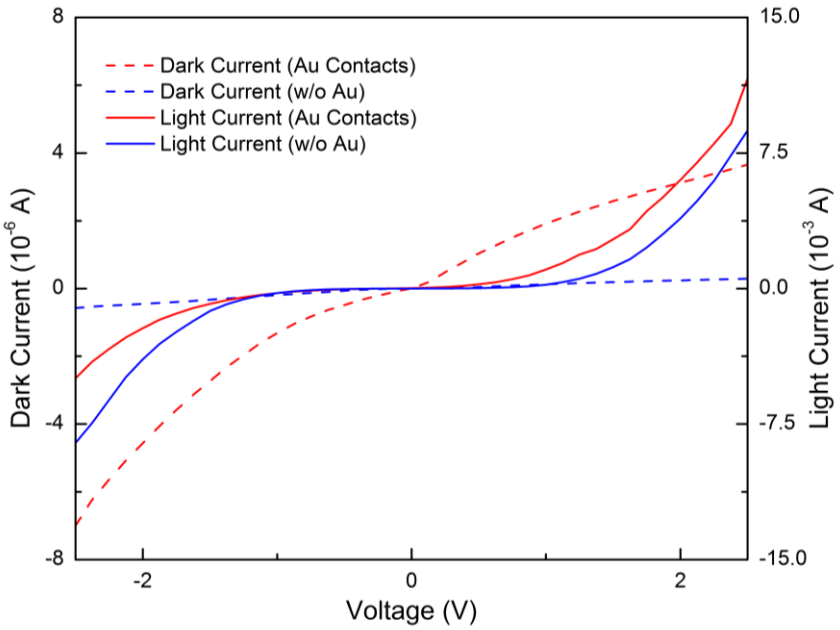

Fig. 11: *Comparison of I-V data (Light Current is under broadband illumination)*

From collected I-V data, it is revealed that the increase in quality of electrical contact and improvement of the power density of the source generates significantly higher responses in the sample. In comparing the developed methods for establishing contact, both dark and light current data indicate that the increased conductivity of the system as a result of Au sputtering increases the signal response. Of note is the asymmetry of the curve, as current flow should hypothetically be symmetric in either direction. This behavior can be associated with the diode-like properties of crystalline Si, although the magnitudes of each curve at the maxima indicate that the direction of the pseudo-diode switches one excitation, as dark current shows higher magnitude under negative voltage whereas light current shows higher magnitude in positive voltages.[3,8]

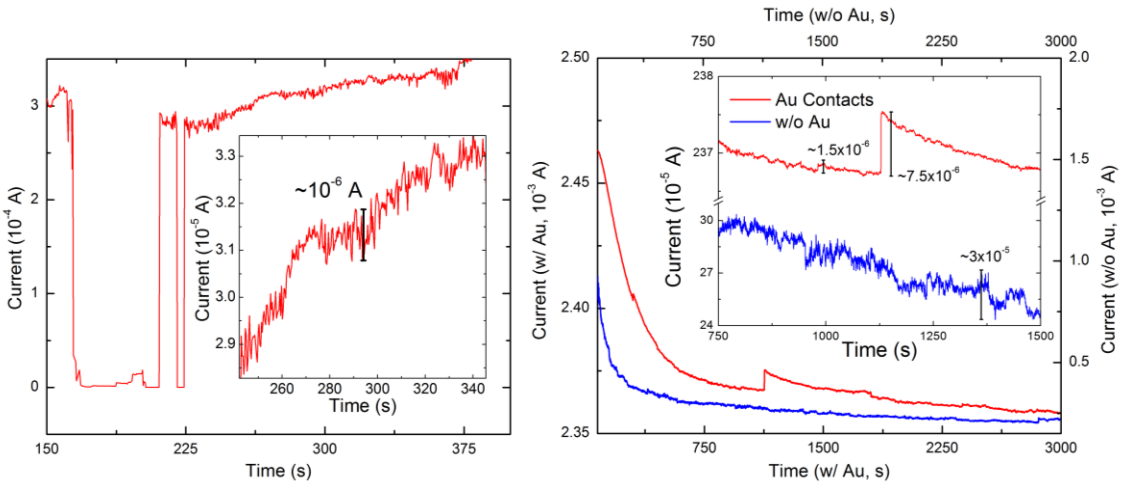

Fig. 12: *(left) common noise in original probe-based measurenents (right) Comparison of various forms of noise in solid contacts (note: All measurements show are under broadband illumination).*

From the time dependent data shown, several conclusions can be drawn pertaining to sources of noise in the various forms of measurement shown and hypotheses as to the remaining sources of fluctuations in current can be developed. Most noticably, sharp losses in conductivity resulting from a loss in contact between probes and gold leads has been entirely eliminated, as can be seen when comparing the lack of sharp drops in current in the right figure versus the significant loss at ~160 seconds in the left figure. It is important to note here that contact was reestablished in the left figure by lowering the leads slightly to compensate for the removal of gold material under the probe. The primary goal of the figure is to show the change in magnitude of current across the Si sample at the voltage applied, as usage of Ag epoxy allowed for signals an order of magnitude higher using one eighth the voltage, as the original data was taken at 20 V, whereas recent data was collected at 2.5 V. Analyzing the features marked with scale bars, it can be noted that the magnitude of seemingly random noise is actually increased by a factor of three in the bare Si sample; this however, is deceptive, as the signal to noise ratio reveals this to be a reduction in effective noise by a factor of three. However, this reduction is drastically overcome with the usage of Au leads and silver epoxy, with this same noise being 1/20th the magnitude in a

signal with 7 times the magnitude. However, there are also apparent instantaneous spikes in conductivity in Au-sputtered data, which are theorized to be related to the relationships in the differential conductivity of Ag, Au, and Si/Schottky barrier effects and differential charge buildup in the sample below Ag-Si and Ag-Au-Si junctions. The first set of explanations rests on the scattering of electrons when passing between two media of different resistivities, resulting in variance in the hypothetical "path of least resistance." This analogy can be extended to the second explanation, as charge buildup beneath each junction would occur at different rates, creating a region of low conductivity and forcing charge carriers to overcome the Shottky barrier at the Ag-Si junction until charge can be dissipated. This could result in the apparent spikes in conductivity as it can be theorized that current would flow quickly across the Ag-Au-Si junction, esstablishing an area of high charge density, resulting in a switching of current into the Ag-Si junction as charge is slowly dissipated. Once this charge is sufficiently depleted, current instantaneously switches into the Ag-Au-Si junction and regenerates said charge buildup, resulting in fast initial switching and a slow relaxation time to the base conductivity. Of note is that this effect is one-quarter of the magnitude of random noise apparent in the bare Si sample, indicating that sputtering gold contacts, in spite of this variance, is a more effective technique for establishing electrical contact in photoconductivty measurements.

Remaining noise in time dependent measurements can be attributed to thermal noise resulting from irradiation of the sample with a high-intensity beam and inherrent in room temperature measurement, imperfections in electrical contacts, and, when considering higher frequency noise not readily identifiable at the resolution available, shot noise, G-R noise, 1/f / $1/f^2$ noise, and burst noise.[7] While reduction of thermal noise would be via usage of a cryostat, remaining sources can only be eliminated by refinement of techniques for producing electrical

contacts and refinement of the instrument to make use of a lock-in amplifier and a 4-probe measurement.[12]

While the improvements detailed in this thesis have contributed significantly to the sensitivity of the photoconductivity setup and have also allowed for the measurement of photocondocutivity and magnetoresistance for future works in the Musfeldt lab. In particular, recent research has been undertaken on the electronic structure of $NiFe_2O_4$, a known high temperature magnet. This data is detailed below in Fig. 13, and, at the time of writing, is currently in preparation for submission to Nature Materials.

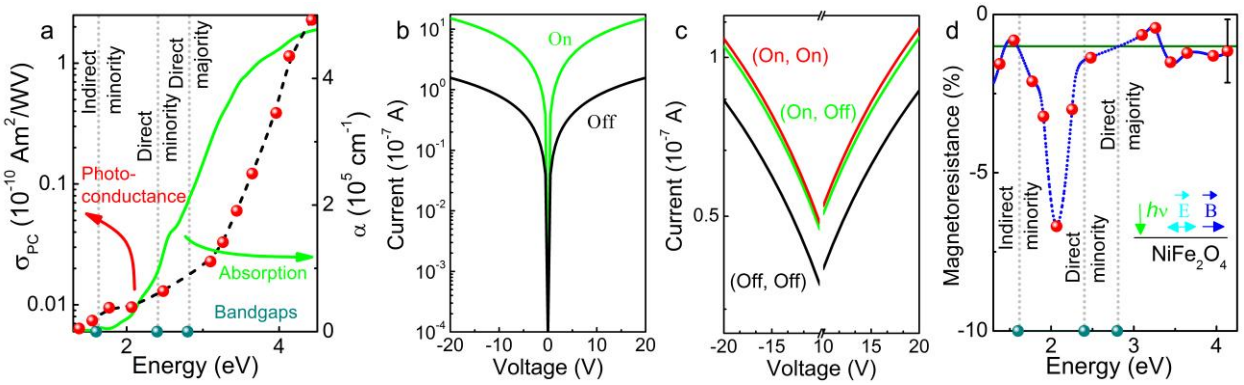

Fig. 13: *Collected data on $NiFe_2O_4$*

Conclusion

In summary, the usage of solid contacts in the measurement of photoconductivity, when coupled with other improvements to the instrument, have succeeded in developing a method by which the instability in time dependent signal can be reduced by three orders of magnitude. Remaining sources of instability require further implementation of methods by which temperature can be controlled and other sources inherent in physical processes be factored out using a lock-in amplifier. If these solutions are implemented, exploration of time dependent processes totally indiscernible to the original instrumentation are now available.

References

1. Bube, Richard H. *Photoconductivity of Solids*. New York: Wiley, 1960.
2. Gilbert, Thomas R., Rein V. Kirss, and Natalie Foster. *Chemistry: An Atoms-focused Approach.* W. W. Norton & Company, 2013.
3. Horowitz, Paul, and Winfield Hill. *The Art of Electronics*. Cambridge: Cambridge University Press, 1989.
4. Kasap, S. O. *Optoelectronics and Photonics: Principles and Practices*. Upper Saddle River, NJ: Prentice Hall, 2001.
5. Kasap, S. O., and Peter Capper. "Photoconductivity in Materials Research." In *Springer Handbook of Electronic and Photonic Materials*, 137-46. New York: Springer, 2006.
6. *Keithley Model 6487 Picoammeter/Voltage Source Reference Manual*. Clevland, OH: Keithley Instruments, 2002.
7. Konczakozska, Alicia, and Bogdan M. Wiliamowski. "Noise in Semiconductor Devices." In *Fundamentals of Industrail Electronics*, 1-12. Boca Raton, FL: CRC Press, 2011.
8. Malvino, Albert Paul. *Electronic Principles*. New York: McGraw-Hill, 1989.
9. Moss, T.S. "Photoconductivity," *Reports on Progress in Physics* 58, no. 1 (1965): 15
10. Padmanabhan, Medini, Kallol Roy, Gopalakrishnan Ramalingam, Srinivasan Raghavan, and Arindam Ghosh. "Electrochemical Integration of Graphene with Light-Absorbing Copper-Based Thin Films." *J. Phys. Chem. C The Journal of Physical Chemistry C* 116, no. 1 (2012): 1200-204. doi:10.1021/jp208120u.
11. Sharma, Surendra, Norbert Weiden, and Alarich Weiss. "Phase Transitions in $CsSnCl_3$ and $CsPbBr_3$ An NMR and NQR Study." *Zeitschrift Für Naturforschung A* 46, no. 4 (1991). doi:10.1515/zna-1991-0406.
12. Smits, F. M. "Measurement of Sheet Resistivities with the Four-Point Probe." *Bell System Technical Journal* 37, no. 3 (1958): 711-18. doi:10.1002/j.1538-7305.1958.tb03883.x.
13. "Thorlabs - Your Source for Fiber Optics, Laser Diodes, Optical Instrumentation and Polarization Measurement & Control." Thorlabs - Your Source for Fiber Optics, Laser Diodes, Optical Instrumentation and Polarization Measurement & Control. Accessed July 14, 2016. https://www.thorlabs.com/tutorials/Tables3.cfm.
14. "Top Performance SmartTable® Table Systems with Hybrid Damping." Top Performance SmartTable® Table Systems with Hybrid Damping. Accessed July 14, 2016. https://www.newport.com/f/smarttable-ots-hd-table-systems-with-hybrid-damping.